Icarus 421 (2024) 116224

Contents lists available at ScienceDirect

Icarus

journal homepage: www.elsevier.com/locate/icarus

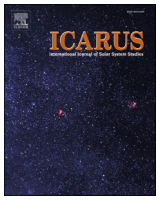

Spatial patterns of valley network erosion on early Mars

Timothy A. Goudge [a,b,*], Alexander M. Morgan [c,d], Gaia Stucky de Quay [e], Caleb I. Fassett [f]

[a] Department of Earth and Planetary Sciences, Jackson School of Geosciences, The University of Texas at Austin, Austin, TX, USA
[b] Center for Planetary Systems Habitability, The University of Texas at Austin, Austin, TX, USA
[c] Planetary Science Institute, Tucson, AZ, USA
[d] Center for Earth and Planetary Studies, National Air and Space Museum, Smithsonian Institution, Washington, DC, USA
[e] Department of Earth, Atmospheric and Planetary Sciences, Massachusetts Institute of Technology, Cambridge, MA, USA
[f] Johns Hopkins University Applied Physics Laboratory, Laurel, MD, USA

ARTICLE INFO

Keywords:
Mars
Valley networks
Landscape evolution

ABSTRACT

Fluvial valley networks are a key record of the geomorphic effects of past liquid water on the surface of Mars. Most valley networks formed early in Mars history (>3.5 Ga) during a period of increased surface water availability, and these landforms may preserve information on the nature and spatial heterogeneity of the ancient martian hydroclimate. Here we present work to constrain patterns of valley network geometry (length, depth, and volume), and assess how these factors are related to topography and landscape position. We find that valley depth is most strongly controlled by regional slope and landscape relief, with deeper valleys on steeper/higher relief terrains, likely driven by a slope control on the rate of fluvial erosion. In contrast, total valley length and volume are most controlled by slope orientation, with larger values on north-draining slopes, which we suggest is related to more efficient fluvial integration (i.e., inter-connection of valleys) on such slopes. At lower elevations and towards terminal basins (northern plains and Hellas), valley depth increases, while total valley length and volume decrease, consistent with the geometry expected as a branching valley system converges downstream into fewer, larger valleys. Finally, we show that patterns of total valley length and eroded volume peak about a previously proposed paleo-latitude band on a pre-Tharsis-driven true polar wander Mars. Valley depth increases from paleo-south to paleo-north in this pre-true polar wander framework, consistent with valley network development in a paleo-north direction. This is potentially consistent with syn/pre-Tharsis growth and true polar wander valley network incision; however, this signal is not unique and may be amplified by patterns of post-valley network incision resurfacing.

1. Introduction

Fluvial valley networks on Mars preserve a record of geomorphic work accomplished by flowing surface water. While recent studies have provided evidence that the process of fluvial valley incision likely occurred throughout much of Mars history (e.g., Howard and Moore, 2011; Wilson et al., 2016; Kite, 2019; Kite et al., 2019; Morgan et al., 2022), it is generally thought that the formation of fluvial valleys was most globally widespread, longest lived, and most intense at or just prior to the Noachian-Hesperian boundary (Howard et al., 2005; Hynek et al., 2010; Fassett and Head, 2008). During this time period of early Mars history, fluvial incision formed branching, often 100s to 1000s of kilometers long systems of valleys referred to as valley networks (e.g., Fig. 1) (Pieri, 1980; Carr, 1987; Howard et al., 2005; Irwin et al., 2008; Hynek et al., 2010).

Although the record of early Mars fluvial valleys is likely incomplete due to post-incision landscape modification (e.g., Irwin and Howard, 2002; Hynek and Phillips, 2003; Matsubara et al., 2013), where they remain exposed, martian valley systems record the time-integrated signal of surface runoff, which is ultimately linked to the early Mars hydroclimate. Therefore, the spatial distribution of valley network characteristics may provide useful constraints on spatial variability of the early Mars hydroclimate.

Indeed, many previous researchers have looked for spatial patterns in the valley network record in an attempt to constrain the early Mars hydroclimate (e.g., Carr and Chuang, 1997; Hynek and Phillips, 2003; Luo and Stepinski, 2009; Hynek et al., 2010; Seybold et al., 2018; Grau Galofre et al., 2020). In most of these past studies, the primary metric

* Corresponding author at: Jackson School of Geosciences, The University of Texas at Austin, 2275 Speedway, Stop C9000, Austin, TX 78712-1722, USA.
E-mail address: tgoudge@jsg.utexas.edu (T.A. Goudge).

https://doi.org/10.1016/j.icarus.2024.116224
Received 23 May 2024; Received in revised form 15 July 2024; Accepted 19 July 2024
Available online 22 July 2024

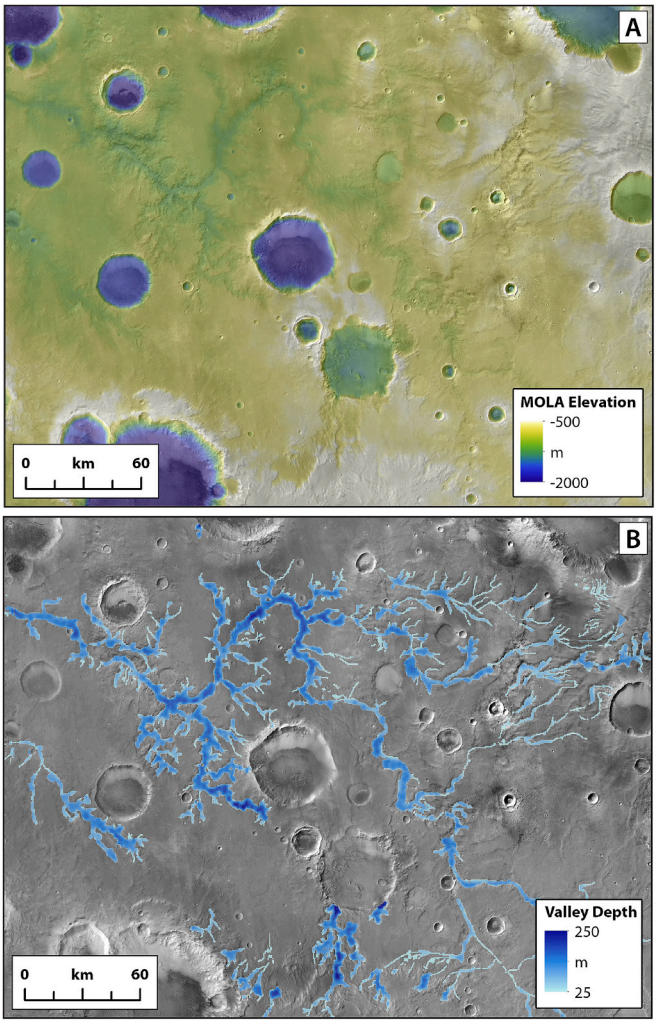

Fig. 1. Example incised valley network system in Noachis Terra. Image is centered at −7.3°N, 2.8°E. **(A)** MOLA gridded topography overlain on the global mosaic (Dickson et al., 2023) of Context Camera (CTX; Malin et al., 2007) images. **(B)** Progressive black top hat-derived valley depth (Luo et al., 2015, 2017; Goudge et al., 2021) overlain on the global CTX mosaic.

used was the valley network line density (total valley length per unit area) or the valley network drainage density (total valley length in a given watershed, normalized by the area of that watershed). These studies have revealed interesting aspects of the early Mars landscape, such as: drainage densities comparable to, although commonly lower than, fluvially dissected landscapes on Earth (Luo and Stepinski, 2009; Hynek et al., 2010); patterns of valley density that do, or do not, match predictions from climate model output (Wordsworth et al., 2015; Bouley et al., 2016; Palumbo and Head, 2018; Guzewich et al., 2021; Kamada et al., 2021); and even possible constraints on the large-scale geophysical evolution of the martian lithosphere (Bouley et al., 2016). While studies of valley network density provide useful information on how the martian landscape has been integrated by surface water in planform, they do not capture the component of vertical incision associated with valley formation, and thus do not provide a complete picture of early Mars fluvial erosion.

In contrast to studies on valley network density, global studies on spatial patterns of valley network depth or volume (which both incorporate information on vertical incision) are relatively rare. For valley network volume, past studies have primarily focused on globally integrated assessments of the total eroded volume of valleys, which have provided planetwide insights into the characteristics and processes of fluvial valley erosion (Rosenberg and Head, 2015; Luo et al., 2017; Rosenberg et al., 2019; Goudge et al., 2021), but not into regional patterns of spatial variation in erosion. Although studies of spatial patterns of valley network depth exist, these primarily focus on small numbers of individual valley systems (e.g., Hoke et al., 2011; Ansan and Mangold, 2013; Orofino et al., 2018), often with the aim of constraining incision timescales (e.g., Hoke et al., 2011; Orofino et al., 2018).

One of the earliest studies of spatial patterns of valley network morphometry looked at variations with respect to latitude, showing that valley depths peak at equatorial latitudes (Williams and Phillips, 2001). While this work provided foundational constraints on the morphometry of martian valley networks, the analyses were conducted using Mars Orbiter Laser Altimeter (MOLA; Smith et al., 2001) point shot data, excluding tracks that crossed near-parallel to valleys. Given the roughly north-south path of MOLA point shot tracks, this biases towards east-west oriented valleys, missing the large number of valleys that flow generally towards the north (Irwin et al., 2011; Luo and Stepinski, 2012). A subsequent study of valley depth using global gridded MOLA data by Luo and Stepinski (2009) confirmed the peak in depths at equatorial latitudes, but again only assessed spatial variations relative to latitude.

The most comprehensive analysis of the spatial variability of valley network depth/volume that the authors are aware of is from Matsubara et al. (2013), who used a hydrologic routing model to define valley network paths and MOLA gridded elevation data to globally assess patterns of valley network depth and eroded volume at a relatively coarse scale (~1000 km/pixel output). One challenge with these results is that the calculated patterns of valley volume and depth are inherently dependent on assumptions of the hydrologic routing model (e.g., assumed climate conditions), although this dependency on model assumptions was fairly weak (Matsubara et al., 2013). Additionally, another concern with these results, as well as those of Luo and Stepinski (2009) and Williams and Phillips (2001), is that they do not distinguish between valley networks (formed by surface runoff) and paleolake outlet canyons (formed by catastrophic lake breach floods; Goudge et al., 2019). Because paleolake outlet canyons are systematically deeper than valley networks (Goudge et al., 2021), this would lead to greater effects in the trends for valley depth and volume than in total valley length (unless valley network and paleolake outlet canyon geometries are also spatially correlated). Still, the results of Matsubara et al. (2013) provide an interesting set of hypotheses to further test, namely that valley depth is most strongly controlled by regional slope, while valley volume is more strongly controlled by discharge, suggesting the latter should be a better proxy for hydroclimate variability.

Here we build on this past work to further constrain the spatial distribution of valley network erosion (including depth and volume) with a new global, observational study of valley geometry patterns. Specifically, we investigate spatial patterns of valley geometry and associations with landscape topography and position. In this paper we first describe our approach (Section 2), followed by a summary of the results of our global analysis (Section 3), and then a discussion of the implications of our results for understanding controls on valley network erosion on Mars (Section 4).

2. Methods

To assess spatial patterns in valley geometry our general approach involved a moving window analysis across the Mars surface using two primary datasets. The first is a vector (line file) map of valley network locations (Fig. 2A), originally compiled by Hynek et al. (2010) and Tanaka et al. (2014) using a combination of topographic and image orbital data. These datasets were merged and further refined by Goudge et al. (2021), removing valleys that post-date the main era of valley network formation, such as those on volcanic edifices (e.g., Gulick and Baker, 1990; Fassett and Head, 2007), as well as paleolake outlet canyons formed by catastrophic lake breach floods (Goudge et al., 2019,

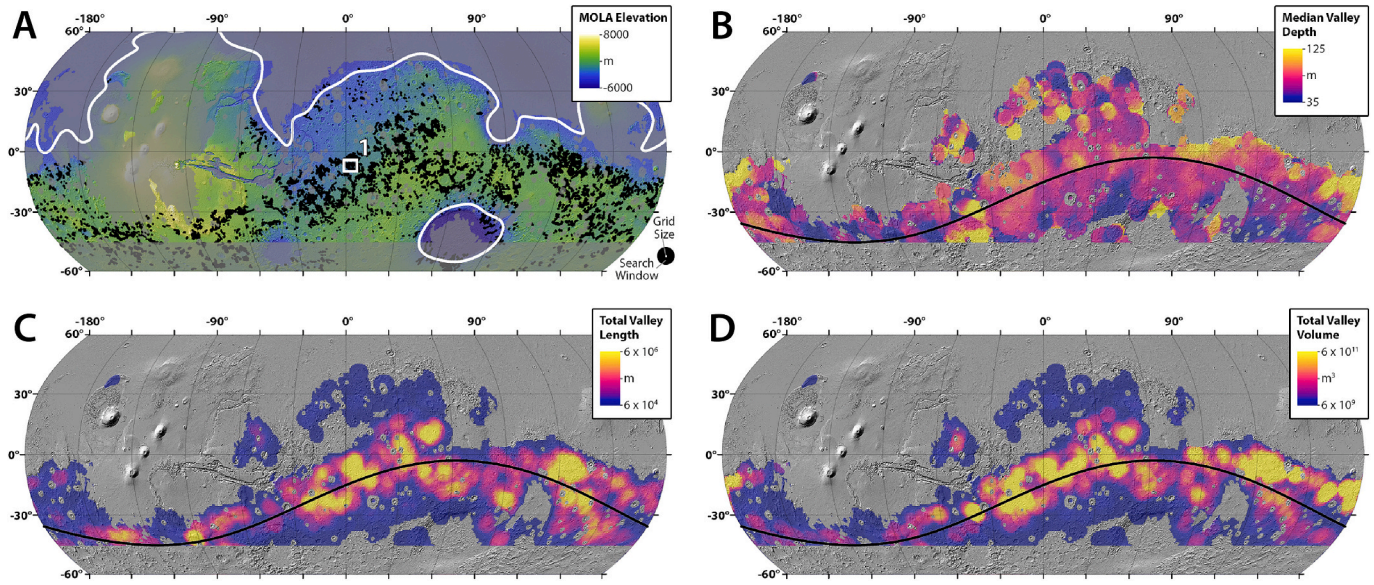

Fig. 2. **(A)** Global distribution of valley networks (black lines). Grey shaded region indicates the combined mask of age (terrain younger than Early Hesperian) and latitude (poleward of ±45°). Thick white line is the −3000 m contour from the degree and order 20 spherical harmonic model of MOLA topography (Black et al., 2017). Background is MOLA gridded topography overlain on MOLA-derived hillshade. Size of the moving search window (250 km radius) and grid cells (50 km) are indicated in the lower right. White box indicates the location of Fig. 1. **(B—D)** Summary of valley geometry within a moving, 250 km radius search window. Background is MOLA-derived hillshade. Thick black line indicates the small circle of high valley network density from Bouley et al. (2016). **(B)** Median valley depth. **(C)** Total valley length. **(D)** Total valley volume.

2021).

The second dataset is a raster (gridded) map of valley network depths associated with the vector map of valley networks. Valley network depths were calculated by Goudge et al. (2021) using the progressive black top hat (PBTH) algorithm of Luo et al. (2015, 2017) and MOLA gridded topography (Smith et al., 2001). The PBTH algorithm searches along a vector map of valleys and identifies the valley shoulder using a progressively widening search window. Depth along the valley can then be calculated as the difference between the valley shoulder and the modern MOLA elevation at each pixel, yielding a map of valley network depth at the same resolution as the MOLA gridded elevation data (~463 m/pixel) (e.g., Fig. 1B).

In addition to these datasets, we assessed landscape characteristics using MOLA gridded topography and the spherical harmonic model of MOLA topography expanded to degree and order 20 from Black et al. (2017). This latter dataset removes short-wavelength contributions to Mars' topographic structure (e.g., small craters), capturing only regional topographic trends at length scales greater than ~530 km (Black et al., 2017). We also created a proxy for the pre-valley topography by adding the PBTH valley depth rasters to the modern MOLA elevation data. While this dataset does not remove the effects of either distributed erosion during the valley network era or post-valley network incision landscape modification, it does eliminate the topographic signature of the valleys themselves.

Using these data we performed a moving window analysis, dividing the martian surface into a grid of cells with a spacing of 50 km in an equidistant cylindrical projection. Although this projection distorts spatial information towards the poles, all calculations during the moving window analysis were conducted in a geodesic framework, meaning the only distortion affecting our dataset is the spacing of grid cells.

At each grid cell we geodesically calculated a 250 km radius circular search window (e.g., Fig. 2A). Within this search window we calculated a variety of valley geometry metrics: the total length of valleys; the total eroded valley volume (i.e., the sum of depth pixels multiplied by the geodesic area of each pixel); and the 50th (median), 75th, 84th, 90th, 95th and 99th percentile valley depth. Within each search window we also used the pre-valley MOLA topography to calculate the average elevation and elevation standard deviation (as a proxy for relief that is relatively insensitive to outliers). Additionally, for each grid cell we calculated the long-wavelength regional slope magnitude and direction by fitting a plane, using linear least squares, to the degree and order 20 spherical harmonic model of MOLA topography extracted from the search window.

Finally, for each grid cell we calculated the shortest geodesic distance to the boundary of one of two terminal basins on Mars: Hellas and the northern plains. For this distance calculation the boundary of these basins was approximated using the −3000 m contour from the degree and order 20 spherical harmonic model of MOLA topography (Fig. 2A, thick white line). For analysis of this metric, any grid cells within the closed contour were omitted. We explicitly note that while both of these basins have been proposed as sites of standing bodies of water (e.g., Baker et al., 1991; Parker et al., 1993; Head et al., 1999; Moore and Wilhelms, 2001; Wilson et al., 2007; Chan et al., 2018), our approach here does not assume the presence of such a body of water. Rather, Hellas and the northern plains are the two largest topographic basins on the martian surface, and thus the two largest terminal basins for draining the southern highlands (Smith et al., 1999). We also note that here we use a straight-line distance to the nearest terminal basin, and not a true flow path distance, and so this metric is best thought of as a proxy for landscape position, indicating whether the grid cell in question is near to, or far from, these ultimate locations for draining water.

To ensure our results focused only on early Mars valley networks, we excluded all grid cells centered on terrain younger than Early Hesperian based on the global geologic map of Tanaka et al. (2014). We also excluded all grid cells centered poleward of ±45°, to reduce the effect of post-valley network, ice-driven landscape modification, which is most prominent at high latitudes (e.g., Kreslavsky and Head, 2000; Mustard et al., 2001; Levy et al., 2014). Finally, we excluded grid cells that had less than or equal to 100 PBTH pixels with non-zero depth values within their search window to reduce outlier-driven noise in patterns of valley depth. This latter constraint only affected ~2% of the data (792 out of 32,635 grid cells), and so is unlikely to have a significant impact on our results.

3. Results

Our moving window analysis reveals patterns of total valley length (Fig. 2C) and total valley volume (Fig. 2D) that have evident spatial structure, following a quasi-sinusoidal pattern (in map view) (Fig. 2C,D, thick black line). Our results on the spatial pattern of total valley length are consistent with past work on patterns of valley network density (e.g., Luo and Stepinski, 2009; Hynek et al., 2010), which is to be expected since our total valley length results are geometrically equivalent to valley network line density as the search window has a uniform area ($\sim 2 \times 10^{11}$ m^2). The spatial patterns of total valley length and volume found here are very similar to a pattern of high valley density fit by a small circle that was noted by Bouley et al. (2016) (Fig. 2C,D, thick black line), which is further discussed in Section 4.2. In contrast to total valley length and volume, median valley depth has a relatively narrow range of values, and the spatial pattern across the southern highlands is more chaotic (Fig. 2B).

Comparing aspects of valley geometry, total valley length and median depth are uncorrelated (Fig. 3A; Table 1), while total valley length and volume are well-correlated, following an approximately linear, positive trend (Spearman correlation coefficient of 0.90) (Fig. 3B; Table 1). Valley depth and valley volume are positively correlated (Fig. 3C; Table 1), although not as strongly as total valley length and volume, and the depth-volume correlation appears to break down at the largest valley depths.

Looking at how valley geometry varies with respect to landscape topography, we find that valley depth is positively correlated with both regional slope (Fig. 4A; Table 1) and elevation standard deviation (Fig. 4B; Table 1). Interestingly, the strength of these correlations, as measured by the Spearman correlation coefficient (ρ), increases when considering larger percentile values of valley depth within the search window (Fig. 5). In other words, the 95th percentile valley depth is more strongly correlated with regional slope and elevation standard deviation than the 75th percentile valley depth.

Total valley length and volume do not have clear relationships with either regional slope or elevation standard deviation (Fig. 4C–F; Table 1). However, looking instead at regional slope direction, we see a clear relationship where both total valley length (Fig. 6B) and volume (Fig. 6C) values are larger on slopes generally towards the north-northwest (and to a lesser degree to the south-southeast). Valley depth is subtly larger on north-directed than on south-directed slopes (Fig. 6A), although the trend is significantly less pronounced than for total valley length or volume.

Finally, looking at trends with landscape position, we first note that distance to the nearest terminal basin and average elevation are well-correlated (Table 1), and both exhibit similar trends with all aspects of valley geometry (Fig. 7). Median depth is negatively correlated with both distance to the nearest terminal basin and average elevation, although the former correlation is notably weaker (Fig. 7A,B; Table 1). Both total valley length and volume show a positive correlation with distance to the nearest terminal basin (Fig. 7C,E; Table 1), and a noisier (especially for valley volume), potential positive correlation with average elevation (Fig. 7D,F; Table 1).

4. Discussion

4.1. Topographic controls on valley geometry

The strong correlation between total valley length and volume (Fig. 3B; Table 1) makes sense when considering the general geometry of martian valley systems, which are typically much longer (order ~10–100s km) than they are deep (order ~10–100s m) or wide (order ~1 km) (Figs. 1–3; Williams and Phillips, 2001; Hynek and Phillips, 2003; Hoke et al., 2011; Ansan and Mangold, 2013; Orofino et al., 2018; Goudge et al., 2021). Therefore, variations in the total length of valleys in a given area (i.e., within our search window) should exert the

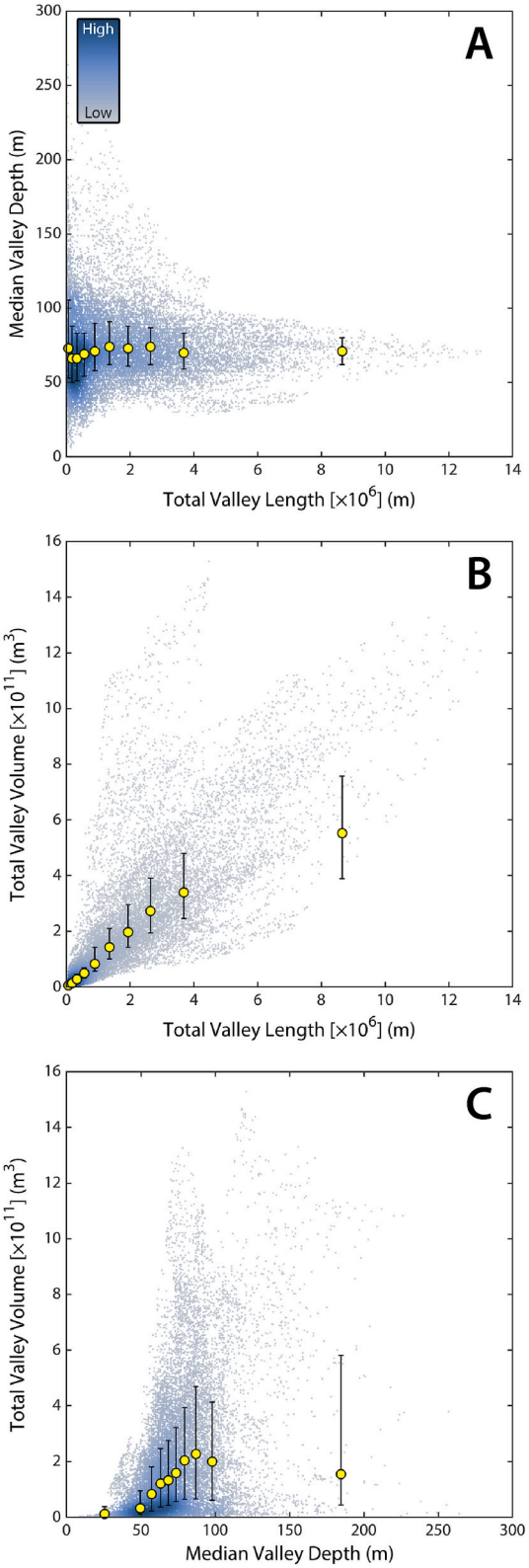

Fig. 3. Relationships between different aspects of valley geometry. **(A)** Median valley depth versus total valley length. **(B)** Total valley volume versus total valley length. **(C)** Total valley volume versus median valley depth. Individual measurements are shown as small points, and are colorized by the kernel density of the data (see relative scale in part **(A)**). Yellow points indicate the median value from decile bins, with the 25th and 75th percentile values for each bin indicated by the error bars. (For interpretation of the references to colour in this figure legend, the reader is referred to the web version of this article.)

Table 1
Spearman correlation coefficient (ρ) for the valley geometry, regional topography and landscape position parameters investigated.

	Total Valley Length	Total Valley Volume	Regional Slope	Elevation Standard Deviation	Distance to Nearest Terminal Basin	Average Elevation
Median Valley Depth	0.03	0.42	0.21	0.19	−0.17	−0.29
Total Valley Length	–	0.90	−0.04	−0.04	0.28	0.31
Total Valley Volume	–	–	0.08	0.07	0.16	0.14
Regional Slope	–	–	–	0.63	−0.24	−0.27
Elevation Standard Deviation	–	–	–	–	−0.21	−0.16
Distance to Nearest Terminal Basin	–	–	–	–	–	0.50

strongest influence on variations in total volume. This also suggests that total valley length is a reasonable proxy of eroded volume, where the latter more completely records the amount of geomorphic work accomplished by fluvial systems on the early Mars landscape, but the former is easier to measure. This finding supports the validity of past work using valley density (equivalent to our measurement of total valley length divided by the search window area, $\sim 2 \times 10^{11}$ m^2) as a metric for assessing spatial variations in fluvial erosion across the martian surface (e.g., Luo and Stepinski, 2009; Wordsworth et al., 2015; Bouley et al., 2016; Palumbo and Head, 2018; Kamada et al., 2021; see further discussion in Section 4.2.).

When considering this result, one important aspect to keep in mind is that total valley length should not be misconstrued as being related to the length of an individual valley system – a search window with a total valley length of 5000 km could just as easily represent a region with 5000 valleys that are each 1 km long or 10 valleys that are each 500 km long. This total valley length metric instead captures how dissected a portion of the Mars landscape is. Since Mars valleys are not observed as numerous, discrete segments, but rather are organized into systems of valley networks (e.g., Fig. 1), the amount of valley dissection is ultimately related to how the early Mars landscape was fluvially integrated (i.e., how valleys connected across the landscape).

Our results are thus consistent with past work suggesting the importance of landscape integration as a limiting factor for early Mars fluvial erosion given the cratered (i.e., disrupted) nature of martian topography (e.g., Irwin and Howard, 2002; Irwin et al., 2011; Luo and Stepinski, 2012; Matsubara et al., 2013; Goudge et al., 2021; Bamber et al., 2022). Furthermore, this conclusion is also consistent with suggestions that periods of fluvial erosion on early Mars were interspersed with periods of ongoing flow path disruption by other surface processes, such as impact cratering, volcanism, or aeolian activity (e.g., Irwin and Howard, 2002; Howard, 2007; Barnhart et al., 2009; Morgan, 2024) due to the intermittent nature of episodes of surface runoff (e.g., Barnhart et al., 2009; Kite, 2019; Stucky de Quay et al., 2021; Wordsworth et al., 2021; Morgan, 2024).

What, then, controlled fluvial landscape integration? One might hypothesize that, since fluvial incision is more efficient on steeper (and higher relief) terrains (Howard and Kerby, 1983; Whipple and Tucker, 1999), fluvial landscape integration should also be most efficient on such terrains. However, our results do not show a clear relationship between total valley length/volume and either regional slope or elevation standard deviation, as a proxy for relief (Fig. 4C–F; Table 1), at least at the measurement scale (250 km radius search window). This suggests any potential relationship between fluvial landscape integration and slope/relief is complex, if it exists at all. One hypothesis that may explain this lack of correlation is that the southern highlands of Mars is a generally steep, high-relief terrain (Smith et al., 1999; Kreslavsky and Head, 1999; Irwin et al., 2011), and so the minimal spatial variation in slope and relief across the surface of Mars may have been insufficient to strongly influence the ultimate patterns of fluvial integration (e.g., Bamber et al., 2022). This hypothesis, while intriguing, requires further work to test, perhaps using a landscape evolution model on different Mars-analog terrains.

Instead, the topographic parameter that appears to have had the most control on total valley length and volume is the orientation of the regional slope (Fig. 6B,C). The long-wavelength topographic structure imposed by the martian dichotomy boundary means that the most continuous slopes on Mars are generally north-draining (Smith et al., 1999; Phillips et al., 2001; Luo and Stepinski, 2012). These long/continuous northward slopes tend to host the longest individual valley systems on Mars (Irwin et al., 2011), implying they were more readily integrated by early martian fluvial processes. Therefore, the larger total valley lengths and volumes on north-draining terrains broadly supports our conclusion that landscape integration was a key control on the amount of fluvial valley erosion across the early martian surface.

In comparison to total valley length and volume, regional slope orientation shows only minimal influence on valley depth (Fig. 6A), while the relationship between valley depth and both regional slope magnitude and relief (elevation standard deviation) shows a clearer, positive trend (Fig. 4A,B; Table 1). This result is consistent with past work on the spatial variability of Mars valley depth (Matsubara et al., 2013).

This correlation may at first seem intuitive when considering theory of bedrock river incision (e.g., the stream power model), where erosion rate is (non-linearly) proportional to slope (Howard and Kerby, 1983; Whipple and Tucker, 1999). However, an important point is that in the stream power model, the landscape slope influences the *rate* of incision, not the ultimate incision depth, which instead is the time-integrated product of the incision rate. Considering this, one potential hypothesis to explain the observed slope-depth correlation is that, globally, valley networks experienced similar incision timescales (i.e., they formed over similar durations of time), allowing the preservation of an incision rate-slope relationship. Following this hypothesis, any variability in depth not accounted for by slope may contain signals of the spatial variability in the early Mars hydroclimate and/or spatial variability in substrate lithology (both laterally and vertically). However, the validity of this hypothesis remains to be further tested.

An additional interesting result from our analysis is the fact that the strength of the correlation between valley depth and regional slope/elevation standard deviation increases when considering larger depth percentiles within the search window (Fig. 5). For example, the slope-depth correlation is stronger when considering the 90th percentile depth in the search window than when considering the median (50th percentile) depth. We propose that this observation reflects the influence of post-valley incision infilling. Since relict fluvial valleys remain as lows on the landscape, they act as traps for sediment over their entire post-incision lifetime (e.g., Goldspiel et al., 1993; Carr and Malin, 2000; Irwin and Howard, 2002; Matsubara et al., 2013), where the amount of infill may be most influenced by latitude and/or substrate lithology (e.g., Gunn et al., 2022). This infilling is likely to skew valley depths to progressively smaller values over time, and thus our reported depths are unlikely to represent initial formative depths. However, unless the amount of infill is positively correlated with the depth of the valley (i.e., deeper valleys have more infill), the amount of infill will have a proportionally larger effect on the measured modern depth of shallower valleys. This proportionally larger effect may thus increase the post-

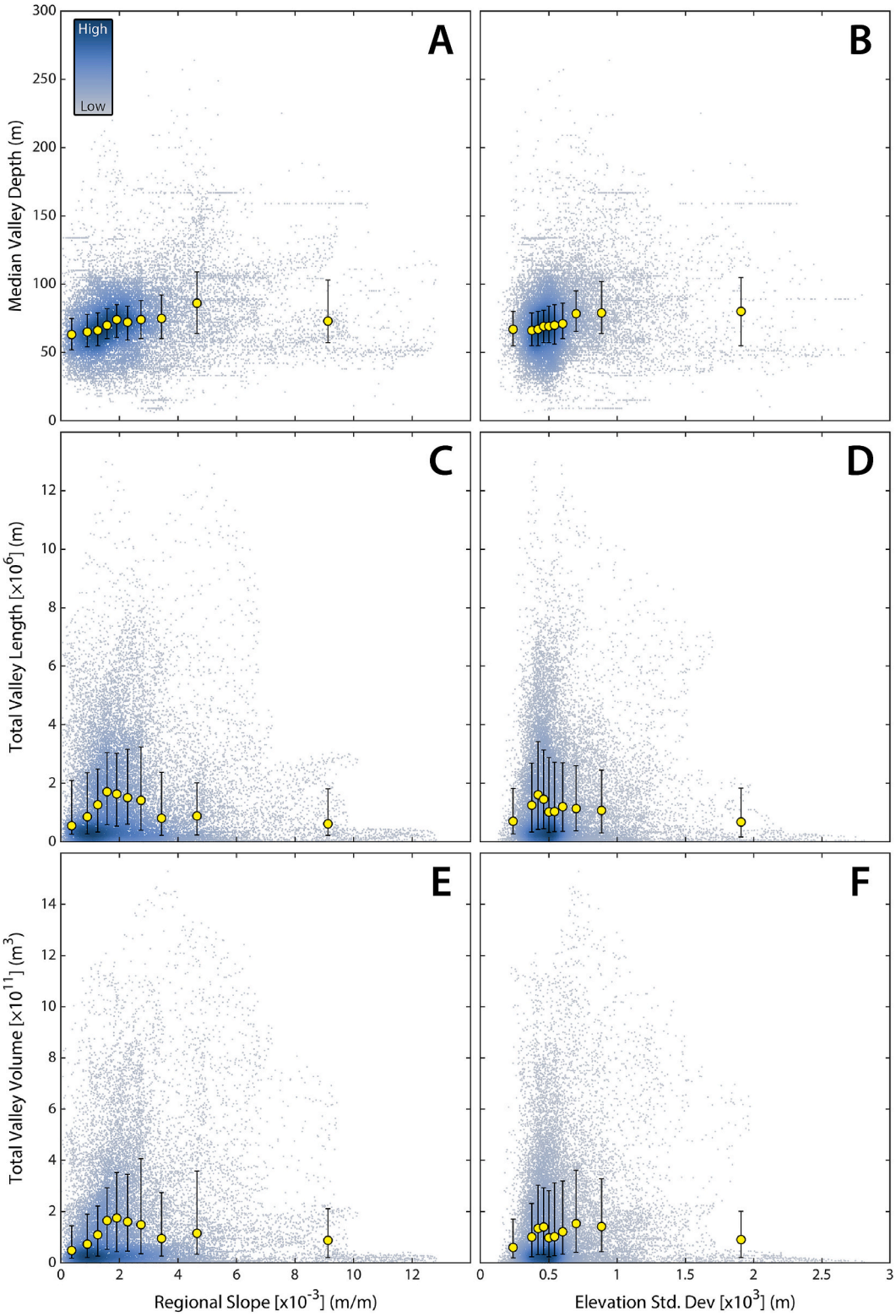

Fig. 4. Relationships between valley geometry and regional topography. Median valley depth **(A),** total valley length **(C)**, and total valley volume **(E)** versus regional slope. Median valley depth **(B),** total valley length **(D)**, and total valley volume **(F)** versus elevation standard deviation. Individual measurements are shown as small points, and are colorized by the kernel density of the data (see relative scale in part **(A)**). Yellow points indicate the median value from decile bins, with the 25th and 75th percentile values for each bin indicated by the error bars. (For interpretation of the references to colour in this figure legend, the reader is referred to the web version of this article.)

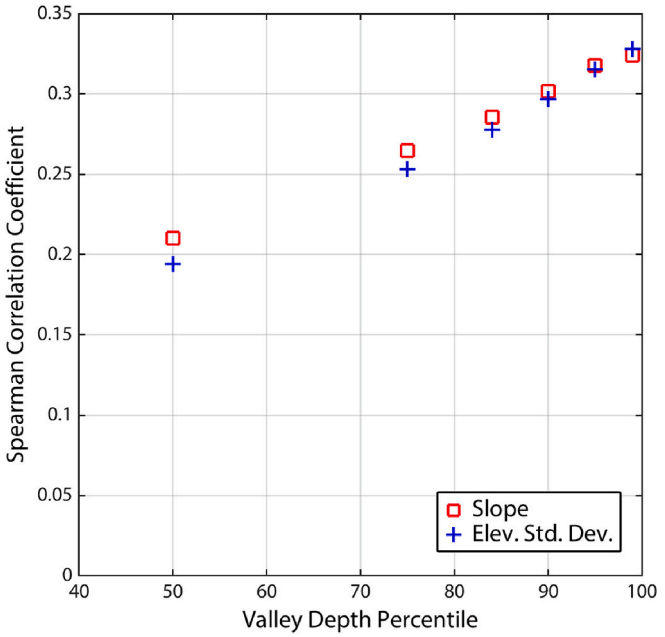

Fig. 5. Spearman correlation coefficient (ρ) calculated for regional slope (red squares) and elevation standard deviation (blue crosses) versus valley depths of varied percentiles, going from 50th (i.e., median) to 99th. (For interpretation of the references to colour in this figure legend, the reader is referred to the web version of this article.)

incisional infilling bias for shallow valleys (i.e., those represented by lower percentile depth values), adding noise to (i.e., weakening) any formative slope-depth or relief-depth correlation. This result also strengthens our conclusion that the slope-depth and relief-depth correlations are related to the formative valley incision process.

4.2. Spatial patterns of valley geometry

Our results also reveal patterns in valley geometry with respect to landscape position, which we have quantified here through distance to the nearest terminal basin (Hellas or the northern plains) and average elevation. We find that valley depth is (slightly) larger and both total valley length and volume are smaller closer to the nearest terminal basin (Fig. 7A,C,E, Table 1). A similar pattern is observed with average elevation, where valleys have a larger depth and smaller total length and volume at lower elevations, although the volume-average elevation trend in particular is quite noisy (Fig. 7B,D,F, Table 1). The similar trend between these landscape position metrics makes sense because the long-wavelength topography of Mars slopes towards Hellas and the northern plains (by nature of their position as terminal basins), meaning that elevation tends to decrease towards these basins, and indeed, these two metrics are correlated (Table 1).

The observation that valleys are deeper, but with less total length (and volume) towards terminal basins (i.e., in the downstream direction) is entirely the expectation of a self-organized river network – as river valleys traverse from upstream catchments towards a terminal sink, they grow into networks through tributary junctions, routing water through fewer but larger valleys downstream (e.g., Leopold and Maddock, 1953; Montgomery and Gran, 2001; Wohl and David, 2008). Therefore, our results of valley geometry changes with respect to landscape position simply point to the branching pattern of Mars valley systems more broadly. While this is the case, we again explicitly note that our results do not provide evidence to support or refute the hypothesis that either of the terminal basins used here previously held standing bodies of water (e.g., Baker et al., 1991; Parker et al., 1993; Head et al., 1999; Moore and Wilhelms, 2001; Wilson et al., 2007; Chan et al., 2018). Valley systems joining and deepening downstream towards a terminal basin is simply a river network expectation, regardless of whether or not that terminal basin contains a standing body of water.

Another interesting observation from these results is that grid cells with the very smallest distances to the nearest terminal basin and at the lowest average elevations (i.e., the 10th percentile bins) show slightly lower median valley depths, breaking from the broader trend (Fig. 7A, B). This could potentially be indicative of a subtle shift from an incisional regime towards a more depositional regime as valleys approach a terminal basin; however, the trend is quite subtle amongst a noisy overall dataset, and so we do not suggest this is a robust observation. It could, however, warrant further research, with an aim to link the patterns of erosional valley networks with ancient depositional river systems that tend to cluster near the margins of both the northern plains and the Hellas basin (e.g., Davis et al., 2016; Cardenas et al., 2018, 2022; Salese et al., 2020; Dickson et al., 2021).

While our observations on the relationship between landscape position and valley geometry conform to the expectation of a branching valley system, these trends are most prominent for valley depth and noisier for total valley length and volume (Fig. 7, Table 1). Additionally, in a simple scenario where valleys join and get deeper downstream, we would expect to see a negative correlation between total valley length and depth. Although the deepest valleys do tend to occur in regions with the smallest total valley lengths (e.g., note the envelope of observations in Fig. 3A), there is no robust correlation between these two geometric variables (Table 1). This suggests other factors could be complicating any potential negative correlation. One complicating factor is the differing topographic controls on valley depth (slope/relief) and total valley length/volume (orientation) (Figs. 4, 6). Regions close to the terminal basin contour used here tend to have steep, north-facing slopes (Fig. 2A, Table 1), which could complicate a potential total length-depth negative correlation for a branched network.

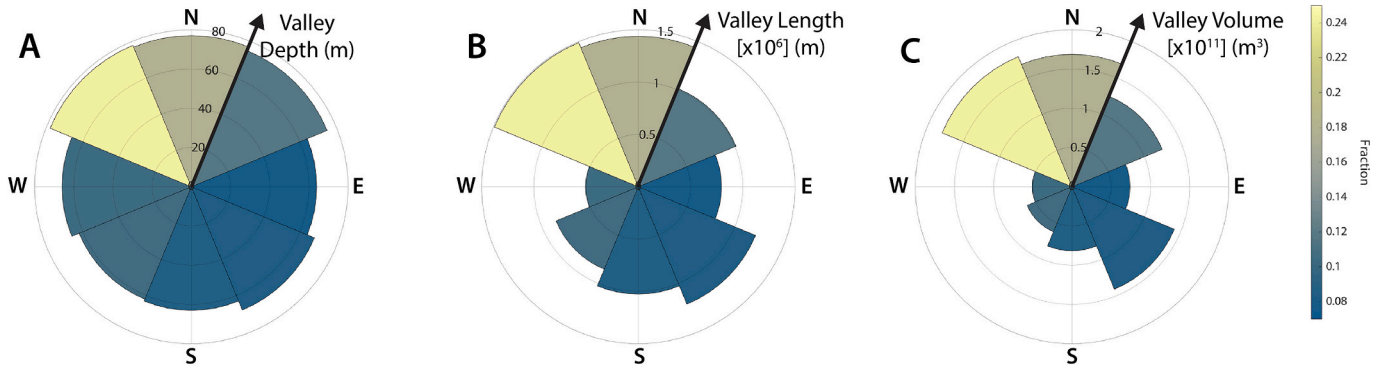

Fig. 6. Polar histograms of the median value of median valley depth **(A)**, total valley length **(B)**, and total valley volume **(C)** within bins of regional slope direction. Colorbar indicates the fraction of grid cells within each bin (i.e., there are more grid cells with north-facing slopes).

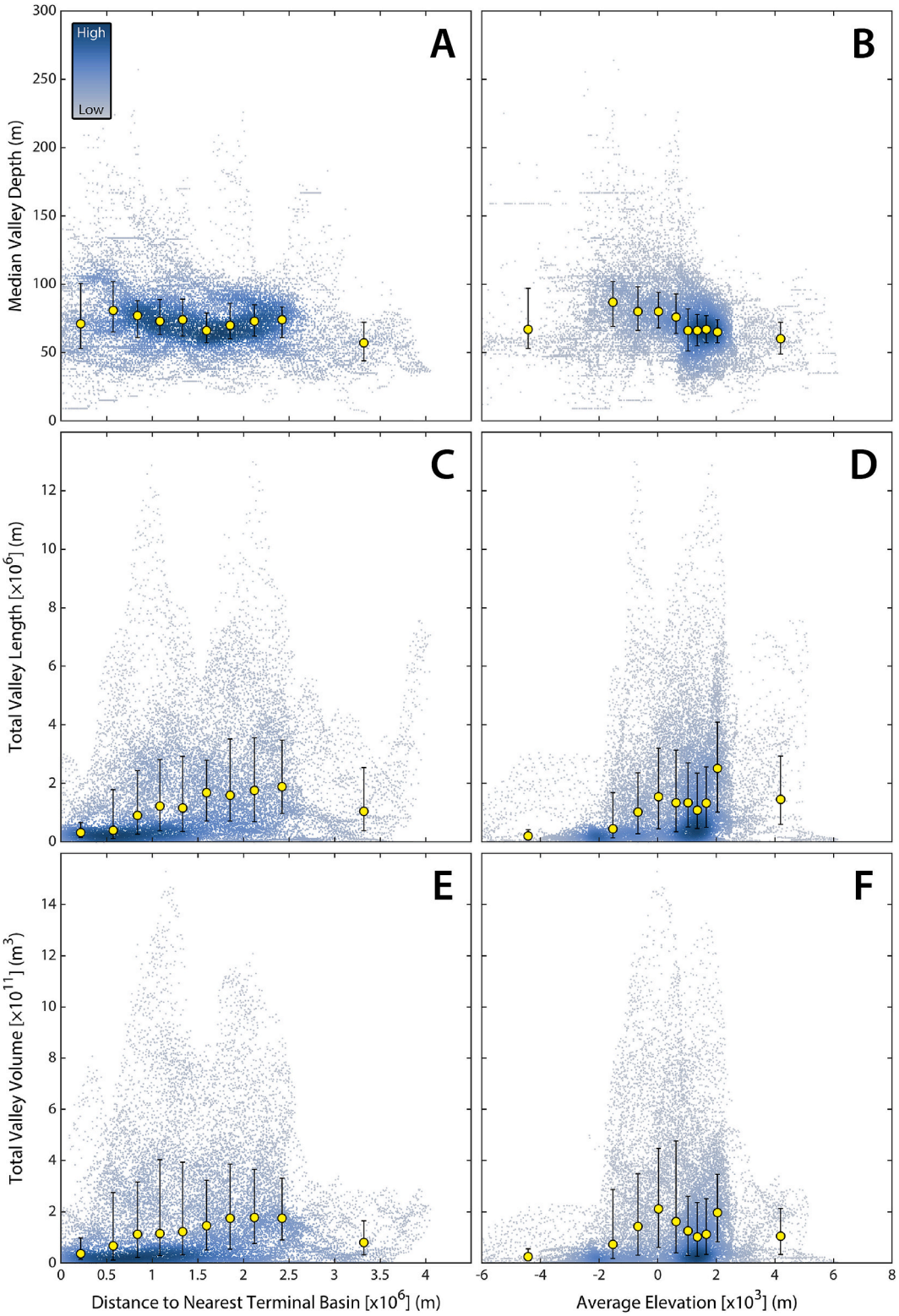

Fig. 7. Relationships between valley geometry and landscape position. Median valley depth **(A),** total valley length **(C)**, and total valley volume **(E)** versus distance to the nearest terminal basin (northern plains or Hellas) (Fig. 2A, thick white line). Median valley depth **(B),** total valley length **(D)**, and total valley volume **(F)** versus average elevation. Individual measurements are shown as small points, and are colorized by the kernel density of the data (see relative scale in part **(A)**). Yellow points indicate the median value from decile bins, with the 25th and 75th percentile values for each bin indicated by the error bars. (For interpretation of the references to colour in this figure legend, the reader is referred to the web version of this article.)

Another important factor to consider when assessing the spatial patterns of our valley geometry results is any potential controls by spatial variability in the early Mars hydroclimate. Indeed, past work has focused much attention on the spatially coherent signal of valley network density (equivalent to our metric of total length; Fig. 2C) to hypothesize this pattern records a signal of spatial variability in the ancient martian hydroclimate, where regions with denser valley networks nominally experienced more surface runoff (e.g., Luo and Stepinski, 2009; Hynek et al., 2010; Wordsworth et al., 2015; Bouley et al., 2016; Palumbo and Head, 2018; Kamada et al., 2021). Our result showing that total valley length is a robust proxy for valley volume (Fig. 3B, Table 1), and thus a robust proxy for how much fluvial erosion was accomplished on the early Mars landscape, may support the hypothesis that spatial patterns in valley density record spatial variability in the ancient martian hydroclimate.

However, this hypothesis implicitly assumes that the relationship between climate (typically precipitation, either rainfall or snow accumulation and melt) and drainage density is monotonic and positive. On Earth, the relationship between valley density and climate is complex (e.g., Abrahams, 1984; Abrahams and Ponczynski, 1984; Moglen et al., 1998), with potentially multiple, opposite-sense relationships depending on the climate environment and soil cover. Such relationships are also inextricably linked with vegetation effects on Earth (e.g., Abrahams and Ponczynski, 1984; Collins and Bras, 2010; Sangireddy et al., 2016), making applicability to Mars unknown. On Mars, there is also a distinct complication of the difficulty in integrating the cratered landscape (e.g., Irwin and Howard, 2002; Irwin et al., 2011; Luo and Stepinski, 2012; Matsubara et al., 2013; Goudge et al., 2021; Bamber et al., 2022), which we suggest is a prominent control on developing heavily-dissected terrain (i.e., with high drainage density). More work is thus needed to develop a mechanistic understanding of the relationship between climate, landscape integration, and valley drainage density on Mars.

Despite these uncertainties, it is worth at least considering how the results presented here might inform our understanding of the spatial variability of the early martian hydroclimate. The most prominent spatial pattern in valley geometry that emerges from our results is a quasi-sinusoidal (in map-view) pattern of high total valley length and volume (Fig. 2C,D, thick black line). This is similar to a spatial pattern of high valley density previously noted and studied in detail by Bouley et al. (2016), who found that this pattern is well-fit by a small circle with a center at ~62°E and ~69°S. Intriguingly, Bouley et al. (2016) note that this center point is coincident with a paleo-south pole location proposed by Matsuyama and Manga (2010) for pre-Tharsis-growth Mars, where the planetary spin axis would have been controlled by the topography of the dichotomy boundary (which would orient parallel to the equator). In this scenario, the emplacement of the large load from the growth of the Tharsis plateau drove true polar wander (TPW), reorienting Mars' lithosphere so that the Tharsis plateau lies along the equator (Matsuyama and Manga, 2010).

In the pre-TPW framework of Mars' crust, the Bouley et al. (2016) small circle of high valley density is a paleo-latitude at 24°S, with most valley networks falling within a band ±14° from this paleo-latitude. Furthermore, Bouley et al. (2016) show that, using pre-TPW and pre-Tharsis topography, this paleo-latitudinal band in Mars' southern hemisphere is also a region of enhanced precipitation (snowfall and accumulation) in climate model output. Therefore, Bouley et al. (2016) hypothesize that the majority of the growth of the Tharsis plateau (and subsequent TPW) occurred contemporaneous with and/or subsequent to the era of valley network incision, a provocative hypothesis given that the Tharsis plateau is typically viewed as an ancient feature of Mars' geology (e.g., Phillips et al., 2001; Rouby et al., 2008).

How do our results of valley geometry fit with this scenario of syn/pre-Tharsis growth and TPW valley network incision? To test this question, we calculated the geodesic distance between each grid cell in our search area and the small circle of high valley density from Bouley et al. (2016). We then converted these distances to a pre-TPW paleo-latitude using the Bouley et al. (2016) small circle paleo-latitude of 24°S, and the assumption of a spherical Mars with a radius of 3,396,190 m. Results of this analysis reveal that total valley length shows a relatively symmetric distribution centered near 24°S (Fig. 8C). This result is expected intuitively based on the qualitative spatial correlation between total valley length and the Bouley et al. (2016) small circle (paleo-latitude) (Fig. 2C, thick black line). Additionally, we quantitatively expect this result because the Bouley et al. (2016) small circle was originally defined as a best-fit to valley density, which is equivalent to our metric of total valley length, albeit at different grid size, search window size, and with a different valley network database. Given the strong correlation between total valley length and total valley volume (Fig. 3B; Table 1), it is equally unsurprising that total valley volume follows a similar symmetric pattern about a paleo-latitude of 24°S (Fig. 8E).

When looking at valley depth, we find a clear positive trend, where valley depth increases from paleo-south to paleo-north in a pre-TPW framework (Fig. 8A). We consider this pattern surprising given the otherwise chaotic spatial pattern of valley depth (Fig. 2B), and because the original definition of the pre-TPW framework by Bouley et al. (2016) relied only on fitting a small circle to valley density and in no way involved valley depth. However, we suggest that this result is indeed consistent with the scenario of enhanced surface runoff and valley network development in a paleo-latitudinal band centered at 24°S, as proposed by Bouley et al. (2016). Our reasoning for this conclusion follows similar logic for the opposite-sense trend of total valley length/volume and depth with respect to distance to the nearest terminal basin, where there are fewer, but deeper, valleys towards a terminal basin (i.e., the sink for a valley system). However, in this case we are now considering the source of these systems (i.e., a paleo-latitude band of enhanced surface runoff), away from which we should see valley depth increase while total valley length decreases.

In the pre-Tharsis-driven TPW framework, the long-wavelength slope of the southern highlands is still directed north towards the dichotomy boundary (Bouley et al., 2016). If one considers the densest, upstream early Mars valleys forming in a paleo-latitudinal band centered near 24°S (due to enhanced surface runoff), we would expect valleys to be shallowest in the upstream portions of catchments (i.e., generally to the paleo-south) and deepest in downstream portions of catchments (i.e., generally to the paleo-north), as is observed (Fig. 8A). Therefore, we suggest that our spatial analysis of valley network geometry is potentially consistent with the hypothesis of Bouley et al. (2016) for syn/pre-Tharsis plateau growth and TPW valley network incision.

Since the above analysis considers trends in valley geometry with respect to paleo-latitude, it seems prudent to also consider any potential trends with respect to modern latitude. When comparing our geometry results to latitude, we find that total valley length and volume somewhat peak near ~10°S (Fig. 8D,F), although this trend is noisier than the pattern with respect to paleo-latitude (Fig. 8C,E). Indeed, looking at the density of points within the full dataset, we mostly observe an increased spread in total valley length and volume from ~20°S to 10°N, which gives the appearance of a peak when taking latitude-binned averages (Fig. 8D,F). In contrast, valley depth shows a more well-defined pattern with respect to modern latitude, with depth increasing northward before peaking near the equator, then declining (Fig. 8B). This pattern of valley depth peaking near the equator is also consistent with past work on latitudinal trends in valley depth (Williams and Phillips, 2001; Luo and Stepinski, 2009), and does make drawing strong conclusions from the trend with (possible) paleo-latitude somewhat more tenuous.

When assessing the trends between valley geometry and paleo-latitude, we also note that the potential for a signature of the Bouley et al. (2016) TPW scenario in the spatial distribution of valleys on modern Mars' surface has recently been called into question. Specifically, Kite et al. (2022) suggest that spatially heterogeneous post-valley network resurfacing can alone explain the quasi-sinusoidal pattern of valley distribution on modern Mars. To test this hypothesis, Kite et al.

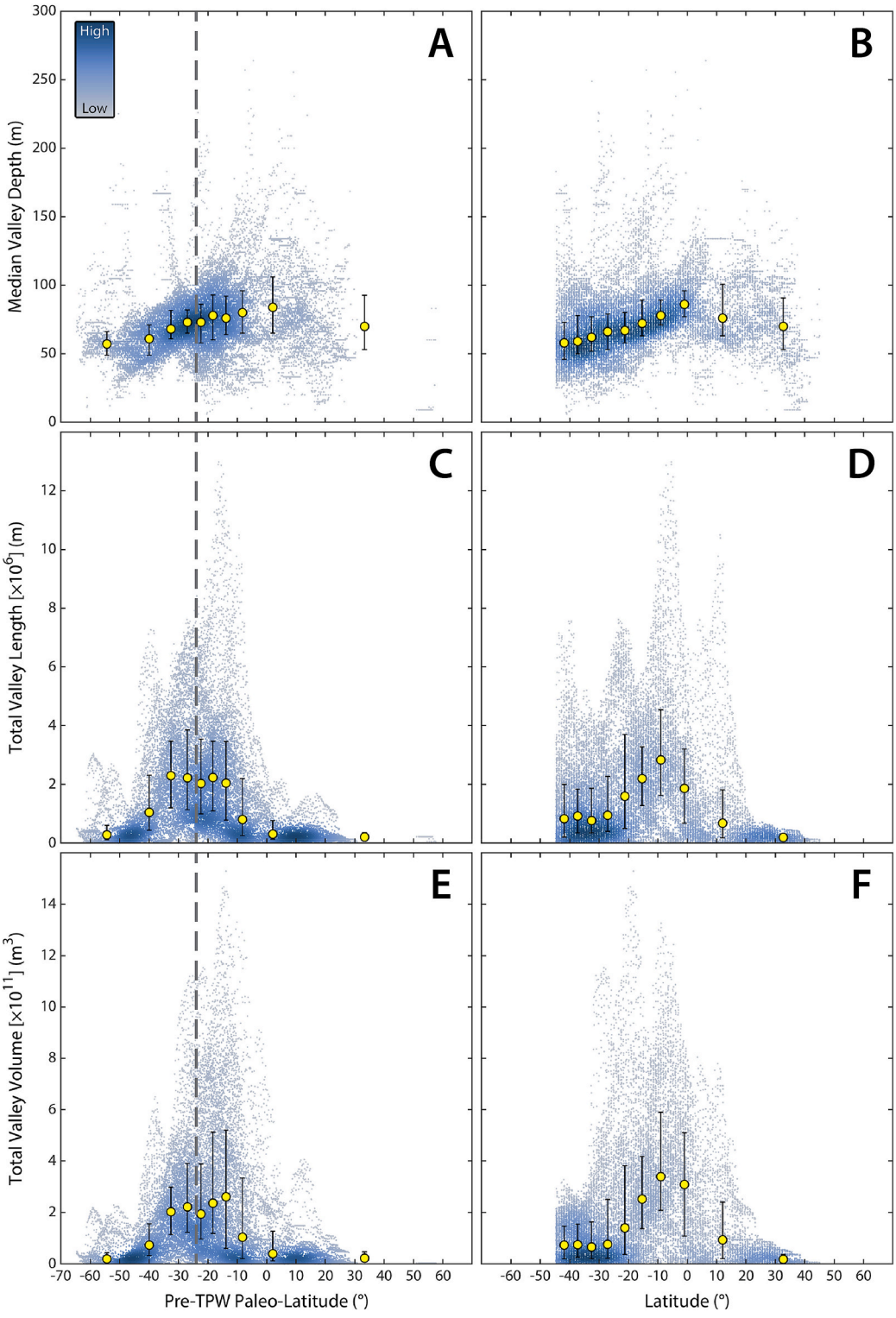

Fig. 8. Relationships between valley geometry and latitude. Median valley depth **(A),** total valley length **(C)**, and total valley volume **(E)** versus paleo-latitude in a pre-Tharsis-driven true polar wander (TPW) framework. Vertical dashed line indicates the center of the paleo-latitudinal band of high valley network density at 24°S from Bouley et al. (2016). Median valley depth **(B),** total valley length **(D)**, and total valley volume **(F)** versus modern latitude. Individual measurements are shown as small points, and are colorized by the kernel density of the data (see relative scale in part **(A)**). Based on the grid-nature of our results, cells in the same grid row share the same modern latitude, so individual measurements of latitude in parts **(B)**, **(D)**, and **(F)** have had ±0.2° of uniform random noise added to aid visualization. Yellow points indicate the median value from decile bins, with the 25th and 75th percentile values for each bin indicated by the error bars. (For interpretation of the references to colour in this figure legend, the reader is referred to the web version of this article.)

(2022) fit a small circle to an artificial dataset of uniformly distributed valley density across terrain that has not been resurfaced subsequent to valley network activity. This fitting yielded a small circle centered at ~58°E and ~79°S, similar to the center-point for the Bouley et al. (2016) best-fit small circle (~62°E, ~69°S).

Based on this result, Kite et al. (2022) argue that the Bouley et al. (2016) best-fit small circle to valley density is a spurious result that is primarily controlled by the spatial distribution of terrain that has, or has not, been resurfaced subsequent to valley network incision. However, this conclusion cannot fully explain the symmetric distribution of total valley length and volume that we observe to peak about a paleo-latitude of 24°S (Fig. 8C,E), nor the systematic increase of valley depth in a paleo-northward direction (Fig. 8A), although we agree that post-valley network resurfacing has likely amplified this signal. Overall, we suggest that our results are at least consistent with the Bouley et al. (2016) hypothesis of syn/pre-Tharsis plateau growth and TPW valley network formation, although perhaps not uniquely so given the complications of post-valley network resurfacing and trends with modern latitude. Still, future work to understand spatial variability in early Mars fluvial activity and hydroclimate should take serious consideration of this TPW scenario.

5. Conclusions

Using a global moving window analysis, we calculate spatial patterns of the geometry of martian valley networks. Total valley length and volume are highly correlated, while total valley length and median depth are uncorrelated (Fig. 3). Although this is the geometric expectation, since martian valleys are much longer than they are deep (or wide), we conclude that this indicates the largest control on fluvial erosion on early Mars was how much the landscape could be integrated in planform, which was likely controlled by the cratered topography of the martian surface. Additionally, our results suggest that that total valley length (and its equivalent drainage density) can be taken as a reasonable proxy for fluvial landscape erosion on Mars, supporting past work using this metric to assess spatial variability in martian fluvial activity.

Valley depth is correlated with both regional slope and relief (Fig. 4A,B), where deeper valleys occur on steeper, higher relief terrain. Since slope is a first order control on incision rate in bedrock valleys, and since ultimate valley depth is the time-integrated product of incision rate, we hypothesize that, globally, valley networks on Mars were active for similar incision timescales (i.e., durations). In contrast to depth, the strongest topographic control on total valley length and volume is slope orientation (Fig. 6B,C), with higher values on north-draining slopes. Given the overall topographic structure of Mars, north-draining slopes tend to be the most continuous (Fig. 2A), consistent with the idea that long/continuous slopes most easily allowed for valley integration across the cratered landscape. We also find that valley depth increases, while total valley length and volume decrease, at lower elevations and towards large terminal basins (northern plains and Hellas) (Fig. 7). We conclude that this is simply a signature of the branching geometry of these valley systems that grow downstream into fewer, but larger valleys.

A final interesting spatial pattern we identify in our data is the alignment between total valley length and volume with a small circle previously noted as a zone of high valley density by Bouley et al. (2016) (Figs. 2, 8). Bouley et al. (2016) hypothesized that this small circle represents the center of a paleo-latitudinal band of enhanced surface runoff in a pre-Tharsis-growth-driven true polar wander Mars, thus explaining the high valley density. We further find that valley depth increases across this paleo-latitude band (Fig. 8A), consistent with valley network growth from paleo-south to paleo-north. However, this signal may be amplified by post-valley network resurfacing that biases towards terrain in a similar spatial pattern (Kite et al., 2022). We suggest that our results are consistent with the hypothesis proposed by Bouley et al. (2016), where Tharsis-growth-driven true polar wander occurred during or subsequent to valley network incision, although may not be uniquely diagnostic.

CRediT authorship contribution statement

Timothy A. Goudge: Visualization, Validation, Methodology, Investigation, Formal analysis, Data curation, Conceptualization, Writing – original draft. **Alexander M. Morgan:** Methodology, Writing – review & editing. **Gaia Stucky de Quay:** Writing – review & editing. **Caleb Fassett:** Writing – review & editing.

Declaration of competing interest

The authors declare that they have no known competing financial interests or personal relationships that could have appeared to influence the work reported in this paper.

Data availability

All moving window analysis results produced here will be have been archived through the Texas Data Repository and are available at https://doi.org/10.18738/T8/LHPHC3.

Acknowledgements

We thank Dr. Seiji Sugita for editorial handling, and two anonymous reviewers for constructive comments that improved the quality and clarity of this manuscript. TAG thanks members of the UT Planetary Surface Processes group and Edwin Kite for valuable discussions and feedback. GSDQ acknowledges financial support from NASA MDAP grant 80NSSC22K0836. AMM acknowledges financial support from NASA MDAP grant 80NSSC17K0454 and SSW grant 80NSSC21K0184. TAG acknowledges financial support from the CIFAR Azrieli Global Scholar/Earth 4D program. This is the University of Texas at Austin Center for Planetary Systems Habitability (UT CPSH) contribution #0076.

References

Abrahams, A.D., 1984. Channel networks: a geomorphological perspective. Water Resour. Res. 20, 161–168.
Abrahams, A.D., Ponczynski, J.J., 1984. Drainage density in relation to precipitation intensity in the U.S.a. J. Hydrol. 75, 383–388.
Ansan, V., Mangold, N., 2013. 3D morphometry of valley networks on Mars from HRSC/MEX DEMs: implications for climatic evolution through time. J. Geophys. Res. Planets 118, 1873–1894. https://doi.org/10.1002/jgre.20117.
Baker, V.R., Strom, R.G., Gulick, V.C., Kargel, J.S., Komatsu, G., Kale, V.S., 1991. Ancient oceans, ice sheets and the hydrological cycle on Mars. Nature 352, 589–594.
Bamber, E.R., Goudge, T.A., Fassett, C.I., Osinski, G.R., Stucky de Quay, G., 2022. Paleolake inlet valley formation: factors controlling which craters beached on early Mars. Geophys. Res. Lett. 49 https://doi.org/10.1029/2022GL101097 e2022GL101097.
Barnhart, C.J., Howard, A.D., Moore, J.M., 2009. Long-term precipitation and late-stage valley network formation: landform simulations of Parana Basin, Mars. J. Geophys. Res. Planets 114. https://doi.org/10.1029/2008JE003122. E01003.
Black, B.A., Perron, J.T., Hemingway, D., Bailey, E., Nimmo, F., Zebker, H., 2017. Global drainage patterns and the origins of topographic relief on earth, Mars, and titan. Science 356, 727–731. https://doi.org/10.1126/science.aag0171.
Bouley, S., et al., 2016. Late Tharsis formation and implications for early Mars. Nature 531, 344–347. https://doi.org/10.1038/nature17171.
Cardenas, B.T., Mohrig, D., Goudge, T.A., 2018. Fluvial stratigraphy of valley fills at Aeolis dorsa, Mars: evidence for base-level fluctuations controlled by a downstream water body. Geol. Soc. Am. Bull. 130, 484–498. https://doi.org/10.1130/B31567.1.
Cardenas, B.T., Lamb, M.P., Grotzinger, J.P., 2022. Martian landscapes of fluvial ridges carved from ancient sedimentary basin fill. Nat. Geosci. 15, 871–877. https://doi.org/10.1038/s41561-022-01058-2.
Carr, M.H., 1987. Water on Mars. Nature 326, 30–35.
Carr, M.H., Chuang, F.C., 1997. Martian drainage densities. J. Geophys. Res. Planets 102, 9145–9152.
Carr, M.H., Malin, M.C., 2000. Meter-scale characteristics of martian channels and valleys. Icarus 146, 366–386. https://doi.org/10.1006/icar.2000.6428.
Chan, N.-H., Perron, J.T., Mitrovica, J.X., Gomez, N.A., 2018. New evidence of an ancient martian ocean from the global distribution of valley networks. J. Geophys. Res. 123, 2138–2150. https://doi.org/10.1029/2018JE005536.

Collins, D.B.G., Bras, R.L., 2010. Climatic and ecological controls of equilibrium drainage density, relief, and channel concavity in dry lands. Water Resour. Res. 46 https://doi.org/10.1029/2009WR008615. W04508.
Davis, J.M., Balme, M., Grindrod, P.M., Williams, R.M.E., Gupta, D., 2016. Extensive Noachian fluvial systems in Arabia Terra: implications for early martian climate. Geology 44, 847–850. https://doi.org/10.1130/G38247.1.
Dickson, J.L., Lamb, M.P., Williams, R.M.E., Hayden, A.T., Fischer, W.W., 2021. The global distribution of depositional rivers on early Mars. Geology 49, 504–509. https://doi.org/10.1130/G48457.1.
Dickson, J.L., Ehlmann, B.L., Kerber, L.H., Fassett, C.I., 2023. Release of the global CTX mosaic of Mars: an experiment in information-preserving image data processing. In: 54th Lunar and Planet. Sci. Conf., Abstract 2353.
Fassett, C.I., Head, J.W., 2007. Valley formation on martian volcanoes in the Hesperian: evidence for melting of summit snowpack, caldera lake formation, drainage and erosion on Ceraunius Tholus. Icarus 189, 118–135. https://doi.org/10.1016/j.icarus.2006.12.021.
Fassett, C.I., Head, J.W., 2008. The timing of martian valley network activity: constraints from buffered crater counting. Icarus 195, 61–89. https://doi.org/10.1016/j.icarus.2007.12.009.
Goldspiel, J.M., Squyres, S.W., Jankowski, D.G., 1993. Topography of small martian valleys. Icarus 105, 479–500.
Goudge, T.A., Fassett, C.I., Mohrig, D., 2019. Incision of paleolake outlet canyons on Mars from overflow flooding. Geology 47, 7–10. https://doi.org/10.1130/G45397.1.
Goudge, T.A., Morgan, A.M., Stucky de Quay, G., Fassett, C.I., 2021. The importance of lake breach floods for valley incision on early Mars. Nature 597, 645–649. https://doi.org/10.1038/s41586-021-03860-1.
Grau Galofre, A., Jellinek, A.M., Osinski, G.R., 2020. Valley formation on early Mars by subglacial and fluvial erosion. Nat. Geosci. 13, 663–668. https://doi.org/10.1038/s41561-020-0618x.
Gulick, V.C., Baker, V.R., 1990. Origin and evolution of valleys on martian volcanoes. J. Geophys. Res. 95, 14,325–14,344.
Gunn, A., Rubanenko, L., Lapôtre, M.G.A., 2022. Accumulation of windblown sand in impact craters on Mars. Geology 50, 981–985. https://doi.org/10.1130/G49936.1.
Guzewich, S.D., Way, M.J., Aleinov, I., Wolf, E.T., Del Genio, A., Wordsworth, R., Tsigaridis, K., 2021. 3D simulations of the early martian hydrological cycle mediated by a H_2-CO_2 greenhouse. J. Geophys. Res. 126 https://doi.org/10.1029/2021JE006825 e2021JE006825.
Head, J.W., Hiesinger, H., Ivanov, M.A., Kreslavsky, M.A., Pratt, S., Thomson, B.J., 1999. Possible ancient oceans on Mars: Evidence from Mars orbiter Laster altimeter data. Science 286, 2134–2137. https://doi.org/10.1126/science.286.5447.2134.
Hoke, M.R.T., Hynek, B.M., Tucker, G.E., 2011. Formation timescales of large martian valley networks. Earth Planet. Sci. Lett. 312, 1–12. https://doi.org/10.1016/j.epsl.2011.09.053.
Howard, A.D., 2007. Simulating the development of martian highland landscapes through the interaction of impact cratering, fluvial erosion, and variable hydrologic forcing. Geomorph 91, 332–363. https://doi.org/10.1016/j.geomorph.2007.04.017.
Howard, A.D., Kerby, G., 1983. Channel changes in badlands. Geol. Soc. Am. Bull. 94, 739–752.
Howard, A.D., Moore, J.M., 2011. Late Hesperian to early Amazonian midlatitude martian valleys: evidence from Newton and Gorgonum basins. J. Geophys. Res. 116 https://doi.org/10.1029/2010JE003. E05003.
Howard, A.D., Moore, J.M., Irwin, R.P., 2005. An intense terminal epoch of widespread fluvial activity on early Mars: 1. Valley network incision and associated deposits. J. Geophys. Res. Planets 110. https://doi.org/10.1029/2005JE002459. E12S14.
Hynek, B.M., Phillips, R.J., 2003. New data reveal mature, integrated drainage systems on Mars indicative of past precipitation. Geology 31, 757–760. https://doi.org/10.1130/G19607.1.
Hynek, B.M., Beach, M., Hoke, M.R.T., 2010. Updated global map of martian valley networks and implications for climate and hydrologic processes. J. Geophys. Res. Planets 115. https://doi.org/10.1029/2009JE003548. E09008.
Irwin, R.P., Howard, A.D., 2002. Drainage basin evolution in Noachian Terra Cimmeria, Mars. J. Geophys. Res. Planets 107, 5056. https://doi.org/10.1029/2001JE001818.
Irwin, R.P., Howard, A.D., Craddock, R.A., 2008. Fluvial valley networks on Mars. In: Rice, S.P., Roy, A.D., Rhoads, B.L. (Eds.), River Confluences, Tributaries and the Fluvial Network. John Wiley & Sons, Ltd., West Sussex, England, pp. 419–451. https://doi.org/10.1002/9780470760383.ch19.
Irwin, R.P., Craddock, R.A., Howard, A.D., Flemming, H.L., 2011. Topographic influences on development of martian valley networks. J. Geophys. Res. 116 https://doi.org/10.1029/2010JE003620. E02005.
Kamada, A., Kuroda, T., Kasaba, Y., Terada, N., Nakagawa, H., 2021. Global climate and river transport simulations of early Mars around the Noachian and Hesperian boundary. Icarus 368, 114618. https://doi.org/10.1016/j.icarus.114618.
Kite, E.S., 2019. Geologic constraints on early Mars climate. Space Sci. Rev. 215, 10. https://doi.org/10.1007/s11214-018-0575-5.
Kite, E.S., Mayer, D.P., Wilson, S.A., Davis, J.M., Lucas, A.S., Stucky de Quay, G., 2019. Persistence of intense, climate-driven runoff late in Mars history. Sci. Adv. 5 https://doi.org/10.1126/sciadv.aav7710 eaav7710.
Kite, E.S., Mischna, M.A., Fan, B., Morgan, A.M., Wilson, S.A., Richardson, M.I., 2022. Changing spatial distribution of water flow charts major change in Mars's greenhouse effect. Sci. Adv. 8 https://doi.org/10.1126/sciadv.abo5894 eabo5894.
Kreslavsky, M.A., Head, J.W., 1999. Kilometer-scale slopes on Mars and their correlation with geologic units: initial results from Mars orbiter laser altimeter (MOLA) data. J. Geophys. Res. Planets 104, 21,911–21,924.
Kreslavsky, M.A., Head, J.W., 2000. Kilometer-scale roughness of Mars: results from MOLA data analysis. J. Geophys. Res. Planets 105, 26,695–26,711.
Leopold, L.B., Maddock, T., 1953. The hydraulic geometry of stream channels and some physiographic implications. US Geol. Surv. Prof. Pap. 252, 57 pp.
Levy, J.S., Fassett, C.I., Head, J.W., Schwartz, C., Watters, J.L., 2014. Sequestered glacial ice contribution to the global martian water budget: geometric constraints on the volume of remnant, midlatitude debris-covered glaciers. J. Geophys. Res. Planets 119, 2188–2196. https://doi.org/10.1002/2014JE004685.
Luo, W., Stepinski, T.F., 2009. Computer-generated global map of valley networks on Mars. J. Geophys. Res. Planets 114. https://doi.org/10.1029/2009JE003357. E11010.
Luo, W., Stepinski, T.F., 2012. Orientation of valley networks on Mars: the role of impact cratering. Geophys. Res. Lett. 39 https://doi.org/10.1029/2012GL054087. L24201.
Luo, W., Pingel, T., Heo, J., Howard, A., Jung, J., 2015. A progressive black top hat transformation algorithm for estimating valley volumes on Mars. Comput. Geosci. 75, 17–23. https://doi.org/10.1016/j.cageo.2014.11.003.
Luo, W., Cang, X., Howard, A.D., 2017. New martian valley network volume estimate consistent with ancient ocean and warm and wet climate. Nat. Commun. 8, 15766. https://doi.org/10.1038/ncomms15766.
Malin, M.C., et al., 2007. Context camera investigation on board the Mars reconnaissance orbiter. J. Geophys. Res. Planets 112. https://doi.org/10.1029/2006JE002808. E05S04.
Matsubara, Y., Howard, A.D., Gochenour, J.P., 2013. Hydrology of early Mars: valley network incision. J. Geophys. Res. Planets 118, 1365–1387. https://doi.org/10.1002/jgre.20081.
Matsuyama, I., Manga, M., 2010. Mars without the equilibrium rotational figure, Tharsis, and the remnant rotational figure. J. Geophys. Res. Planets 115. https://doi.org/10.1029/2010JE003686. E12020.
Moglen, G.E., Eltahir, E.A.B., Bras, R.L., 1998. On the sensitivity of drainage density to climate change. Water Resour. Res. 34, 855–862.
Montgomery, D.R., Gran, K.B., 2001. Downstream variations in the width of bedrock channels. Water Resour. Res. 37, 1841–1846.
Moore, J.M., Wilhelms, D.E., 2001. Hellas as a possible site of ancient ice-covered lakes on Mars. Icarus 154, 258–276. https://doi.org/10.1006/icar.2001.6736.
Morgan, A.M., 2024. New maximum constraints on the era of martian valley network formation. Earth Planet. Sci. Lett. 626, 118509 https://doi.org/10.1016/j.epsl.2023.118509.
Morgan, A.M., Wilson, S.A., Howard, A.D., 2022. The global distribution and morphologic characteristics of fan-shaped sedimentary landforms on Mars. Icarus 385, 115137. https://doi.org/10.1016/j.icarus.2022.115137.
Mustard, J.F., Cooper, C.D., Rifkin, M.K., 2001. Evidence for recent climate change on Mars from the identification of youthful near-surface ground ice. Nature 412, 411–414. https://doi.org/10.1038/35086515.
Orofino, V., Alemanno, G., Di Achille, G., Mancarella, F., 2018. Estimate of the water flow duration in large martian fluvial systems. Planet. Space Sci. 163, 83–96. https://doi.org/10.1016/j.pss.2018.06.001.
Palumbo, A.M., Head, J.W., 2018. Early Mars climate history: characterizing a "warm and wet" martian climate with a 3-D global climate model and testing geological predications. Geophys. Res. Lett. 45 https://doi.org/10.1029/208GL079767, 10,249–10,258.
Parker, T.J., Gorsline, D.S., Saunders, R.S., Pieri, D.C., Schneeberger, D.M., 1993. Coastal geomorphology of the martian northern plains. J. Geophys. Res. Planets 98, 11,061–11,078.
Phillips, R.J., et al., 2001. Ancient geodynamics and global-scale hydrology on Mars. Science 291, 2587–2591. https://doi.org/10.1126/science.1058701.
Pieri, D.C., 1980. Martian valleys: morphology, distribution, age, and origin. Science 210, 895–897.
Rosenberg, E.N., Head, J.W., 2015. Late Noachian fluvial erosion on Mars: cumulative water volumes required to carve the valley networks and grain size of bed-sediment. Planet. Space Sci. 117, 429–435. https://doi.org/10.1016/j.pss.2015.08.015.
Rosenberg, E.N., Palumbo, A.M., Cassanelli, J.P., Head, J.W., Weiss, D.K., 2019. The volume of water required to carve the martian valley networks: improved constraints using updated methods. Icarus 317, 379–387. https://doi.org/10.1016/j.icarus.2018.07.017.
Rouby, H., Greff-Lefftz, M., Besse, J., 2008. Rotational bulge and one plume convection patter: influence on martian true polar wander. Earth Planet. Sci. Lett. 272, 212–220. https://doi.org/10.1016/j.epsl.2008.04.044.
Salese, F., McMahon, W.J., Balme, M.R., Ansan, V., Davis, J.M., Kleinhans, M.G., 2020. Sustained fluvial deposition recorded in Mars' Noachian stratigraphic record. Nat. Commun. 11, 2067. https://doi.org/10.1038/s41467-020-15622-0.
Sangireddy, H., Carothers, R.A., Stark, C.P., Passalacqua, P., 2016. Controls of climate, topography, vegetation, and lithology on drainage density extracted from high resolution topography data. J. Hydrol. 537, 271–282. https://doi.org/10.1016/j.jhydrol.2016.02.051.
Seybold, H.J., Kite, E.S., Kirchner, J.W., 2018. Branching geometry of valley networks on Mars and earth and its implications for early martian climate. Sci. Adv. 4 https://doi.org/10.1126/sciadv.aar6692 eaar6692.
Smith, D.E., et al., 1999. The global topography of Mars and implications for surface evolution. Science 284, 1495–1503. https://doi.org/10.1126/science.284.5419.1495.
Smith, D.E., et al., 2001. Mars orbiter laser altimeter: experiment summary after the first year of global mapping of Mars. J. Geophys. Res. Planets 106, 23,689–23,722.
Stucky de Quay, G., Goudge, T.A., Kite, E.S., Fassett, C.I., Guzewich, S.D., 2021. Limits on runoff episode duration for early Mars: integrating lake hydrology and climate models. Geophys. Res. Lett. 48 https://doi.org/10.1029/2021GL093523 e2021GL093523.
Tanaka, K.L., et al., 2014. Geologic Map of Mars. U.S. Geological Survey Scientific Investigations Map SIM 3292. http://pubs.usgs.gov/sim/3292.

Whipple, K.X., Tucker, G.E., 1999. Dynamics of the stream-power river incision model: implications for height limits of mountain ranges, landscape response timescales, and research needs. J. Geophys. Res. 104, 17,661–17,674.

Williams, R.M.E., Phillips, R.J., 2001. Morphometric measurements of martian valley networks from Mars orbiter laser altimeter (MOLA) data. J. Geophys. Res. Planets 106, 23,737–23,751.

Wilson, S.A., Howard, A.D., Moore, J.M., Grant, J.A., 2007. Geomorphic and stratigraphic analysis of crater Terby and layered deposits north of Hellas basin, Mars. J. Geophys. Res. Planets 112. https://doi.org/10.1029/2006JE002830. E08009.

Wilson, S.A., Howard, A.D., Moore, J.M., Grant, J.A., 2016. A cold-wet middle-latitude environment on Mars during the Hesperian-Amazonian transition: evidence from northern Arabia valleys and paleolakes. J. Geophys. Res. Planets 121, 1667–1694. https://doi.org/10.1002/2016JE005052.

Wohl, E., David, G.C.L., 2008. Consistency of scaling relations among bedrock and alluvial channels. J. Geophys. Res. 113 https://doi.org/10.1029/2008JF000989. F04013.

Wordsworth, R.D., Kerber, L., Pierrehumbert, R.T., Forget, F., Head, J.W., 2015. Comparison of "warm and wet" and "cold and icy" scenarios for early Mars in a 3-D climate model. J. Geophys. Res. 120, 1201–1219. https://doi.org/10.1002/2015JE004787.

Wordsworth, R.D., et al., 2021. A coupled model of episodic warming, oxidation and geochemical transitions on early Mars. Nat. Geosci. 14, 127–132. https://doi.org/10.1038/s41561-021-00701-8.